The peculiar bursting nature of CP Pup

M. Veresvarska [1]★, S. Scaringi [1], S. Hagen [1], D. De Martino,[2] C. Done,[1] K. Ilkiewicz [1,3]
C. Knigge [4] and C. Littlefield[5]

[1]*Centre for Extragalactic Astronomy, Department of Physics, Durham University, South Road, Durham DH1 3LE, UK q*
[2]*INAF-Osservatorio Astronomico di Capodimonte, Salita Moiariello 16, I-80131 Naples, Italy*
[3]*Astronomical Observatory, University of Warsaw, Al. Ujazdowskie 4, PL-00-478 Warszawa, Poland*
[4]*School of Physics and Astronomy, University of Southampton, Highfield, Southampton SO17 1BJ, UK*
[5]*Bay Area Environmental Research Institute, Moffett Field, CA 94035, USA*

ABSTRACT

The classical nova CP Puppis has been observed to have particularly puzzling and peculiar properties. In particular, this classical nova displays occasional bursts in its long-term *ASAS-SN* light curve. Here, we report on five sectors of *TESS* data displaying two of these rapid bursts, lasting ∼1 d. Based on the estimated lower energy limits of the bursts, we discuss whether the bursts may be examples of micronovae resulting from localized thermonuclear explosion. Furthermore, its orbital period remains uncertain, with several inconsistent periodic signals appearing in spectroscopic and photometric observations at various wavelengths. Although we cannot unambiguously unravel the physical origin of the signals, the previously suggested nature of CP Puppis as a long orbital period system may be a viable explanation. The recurrence time of the bursts in CP Puppis, together with the unexplained variable modulations make it a prime candidate for intense monitoring.

Key words: accretion, accretion discs – novae, cataclysmic variables
.

1 INTRODUCTION

CP Puppis (CP Pup hereafter) is a well-studied cataclysmic variable that has undergone a nova explosion in 1942. It is an unusually bright and fast example of a nova explosion, with the difference in amplitude of apparent magnitude of ∼17 mag (Payne-Gaposchkin 1964). It is also a particularly fast nova with $t_3 \sim 6.5$ d (Payne-Gaposchkin 1964), where t_3 represents the time it takes for the nova luminosity to decline by 3 mag. It has been reported that since the nova explosion the brightness levels of the nova have yet to return to the pre-burst quiescence level (Schaefer & Collazzi 2010). Similarities can be drawn between CP Pup and V1500 Cyg (Della Valle & Livio 1998), which is also uncharacteristically brighter and has also remained brighter post eruption. CP Pup is also suggested to have a magnetic accretor (Balman, Orio & Ogelman 1995; Orio et al. 2009; Mason et al. 2013).

One of the main peculiarities of CP Pup is its elusive orbital period. There have been spectroscopic (Bianchini, Friedjung & Sabbadin 1985; Duerbeck, Seitter & Duemmler 1987; O'Donoghue et al. 1989; White, Honeycutt & Horne 1993; Bianchini et al. 2012; Mason et al. 2013) and photometric (Warner 1985; O'Donoghue et al. 1989; Diaz & Steiner 1991; White et al. 1993; Bruch 2022) periods reported between 0.06115 and 0.06834 d. A summary of all these is provided in Bruch (2022). Both spectroscopic and photometric periods reported in literature lie in a similar range, with most of the

spectroscopic periods being shorter. Furthermore, the spectroscopic periods have been reported to show large scatter in the folded radial velocity curve (Bianchini et al. 2012). It is worth noting that the spectroscopic and photometric periods in the literature are inconsistent with each other (Diaz & Steiner 1991). Orio et al. (2009) has further reported three periods from *XMM–Newton* data. However, due to the large uncertainty, the periods quoted in Orio et al. (2009) are consistent with each other, as well as consistent with previously reported spectroscopic and photometric periods (see summary by Bianchini et al. 2012 and Bruch 2022).

If taken at face value as the orbital period, all the reported values are short for known classical novae and non-magnetic nova-likes in general (∼3 h), making CP Pup one of a handful of novae with a potential period reported below the period gap (Bianchini et al. 1985; Marelli et al. 2018). It has thus been suggested that CP Pup is a system whose disc is always hot and bright, and often exhibits superhumps, persisting in a state similar to SU UMa type dwarf novae during superoutburst (Warner 1985; Patterson & Warner 1998; Patterson et al. 2013).

Further interpretations of the period assigned it to the spin of the magnetic white dwarf (WD), suggesting a WD slightly out of spin–orbit synchronism (Warner 1985; Diaz & Steiner 1991; Balman et al. 1995). Asynchronous polars are not the only option for the magnetic interpretation of CP Pup. Orio et al. (2009) and Mason et al. (2013) consider the hypothesis of CP Pup being an intermediate polar. However, there is a lack of conclusive evidence for either interpretation.

★ E-mail: martina.veresvarska@durham.ac.uk

Table 1. Summary of the *TESS* data of CP Pup, with sector numbers and dates. If a sector contains a burst, the corresponding date in Barycentric Kepler Julian date, duration in days, and energy is noted. The details of energy calculation are described in Section 3.1.

Sector	Dates (BTJD-2457000)	Burst dates (BTJD-2457000)	Duration (d)	Energy (erg)
7	1491.6–1516.1	1491.6–1492.2	∼0.6	1.2×10^{38}
8	1518.0–1542.0	–	–	–
34	2229.0–2254.1	2229.0–2234.4	∼1	6.3×10^{37}
35	2255.7–2280.0	–	–	–
61	2964.0–2988.1	–	–	–

The peculiar nature of CP Pup extends to other observations too. The relatively recent nova explosion, with its characteristics such as peak absolute magnitude, suggests a high-mass WD, due to the smaller physical accretor size resulting in higher pressure, making it more favourable to trigger a nova explosion (Prialnik & Kovetz 1995). However, White et al. (1993) point out that the reported values of $K_1 \sim 70$–146 kms^{-1} require a WD mass <0.2 M$_\odot$. This is in contradiction to the nova nature of CP Pup. Some more recent studies adopting higher WD mass of 1.1 M$_\odot$ have instead obtained better fits to optical spectra with an accretion rate in the range of 3.3–7.3 $\times 10^{-10}$ M$_\odot$ yr^{-1} (Mason et al. 2013). Also assuming a high-mass WD, $M_{WD} > 1.1$ M$_\odot$, Orio et al. (2009) derived an upper limit on mass transfer rate ≲1.6 $\times 10^{-10}$ M$_\odot$ yr^{-1}. However, this estimate assumes a distance of 1600 pc, more than double the distance of 780 ± 11 pc inferred from the *Gaia* parallax (Gaia Collaboration 2016, 2023). Orio et al. (2009) also quote a 3σ upper limit ≲8 $\times 10^{-11}$ M$_\odot$ yr^{-1} at 850 pc, as determined by Cohen & Rosenthal (1983). Other estimates of the accretion rate adopting the more precise *Gaia* parallax measurement have been made. Selvelli & Gilmozzi (2019) report a considerably higher value of $10^{-9.22 \pm 0.32}$ M$_\odot$ yr^{-1}. This is related to the unusually high extinction of $A_v \sim 0.6$ mag, which they adopt.

In this work, we report on the analysis of five sectors of *TESS* data of CP Pup (Section 2). In Section 3, we discuss two rapid bursts observed as well as the phenomenology of the cluster of periods found in the *TESS* light curves. Reanalysis of *XMM–Newton* data of CP Pup is also discussed here and the new WD mass estimate is derived. In Section 4, we discuss the observed rapid bursts in the context of the micronova model (Scaringi et al. 2022b, c).

2 OBSERVATIONS

The data used in this work were obtained by *TESS* and are available on the Mikulski Archive for Space Telescopes (MAST).[1] *TESS* observed CP Pup over five sectors amounting to ∼5 months of observations at 2 min cadence. The last sector 61 also contains 20 s cadence data. The detailed description of the data with the burst characteristics is provided in Table 1. *TESS* provides two modes for output flux. Here, the SAP flux is used, as opposed to the processed version of PDCSAP. This is to avoid any contamination of the data through pipeline processing. The flux is then cleaned with a mask discarding any data points with quality flag > 0, to mitigate presence of artificial or non-intrinsic features in the data.

The *TESS* data show a modulation of the shape of the light curve in the form of a larger envelope, where the variance and flickering temporarily varies on time-scales of ≲10 d (see Fig. 1). The same envelope is present to a greater extent in the 20 s cadence data of Sector 61 in *TESS*. The Lomb–Scargle periodogram of the 20 s data shows a quasi-periodic oscillation resembling feature at ≈1500 cycles per day. This is also present in all the neighbouring stars in the field of CP Pup and hence assumed to not be intrinsic to the CP Pup itself, but rather a common systematic. Similar behaviour is also observed in other *TESS* 20 s observations in Sector 61 (such as TIC 260266504, TIC 289 113 766, and TIC 289113764). This points to an instrumental origin of the QPO and is hence disregarded. As no other new signals are found in the 20 s cadence data of Sector 61, the 2 min cadence is used throughout for consistency. The data are downloaded and cleaned for cosmic rays through the LIGHTKURVE package.[2]

While *TESS* provides an excellent precision relative photometry, it is better to leverage data from another observatory to obtain absolute photometry from *TESS* data. To convert the *TESS* data to erg s^{-1}, it is necessary to consider ground-based observations as well as knowledge of its distance. Quasi-simultaneous *ASAS-SN* g-band data (Shappee et al. 2014; Kochanek et al. 2017) is used for this purpose. The band is centred at 475 nm with 140 nm width, with a partial overlap with the *TESS* bandpass (600–1000 nm). Although the passbands do not exactly overlap, we here assume that any colour-term variation is minimal. The data are obtained from the *ASAS-SN* webpage.[3] The conversion is done through simultaneous observations for each half sector. Simultaneous data consist of all *ASAS-SN* observations within a *TESS* cadence observation of 2 min. Assuming a linear relation between the two bands a direct conversion can be established in the form of $F_{ASAS-SN}$[mJy] $= A \times F_{TESS}[e^- s^{-1}] + C$. The corresponding values of the coefficients for each half-sector are specified in Table 2 to account for any deviations in data due to the gap in the middle of *TESS* sectors.

There are two cases where the calibration between *TESS* and *ASAS-SN* fails. The first is in Sector 8, where the *TESS* light curve shows a drop in flux inconsistent with the ground-based *ASAS-SN* observations. This is also reported in Bruch (2022). Another similar case occurs in Sector 35 where the *TESS* data show an uncharacteristic rise in flux, but this appears to be shared within the entire region surrounding CP Pup and we attribute this to poor background correction. Consequently both segments of Sectors 8 and 35 where the calibration to *ASAS-SN* fails are discarded. The final result is shown in Fig. 1, where the light curve is also corrected for the distance of 780 ± 11 pc inferred from *Gaia* DR3 parallax. Despite the high extinction in *Gaia* passband, no bolometric correction has been applied. This is to avoid any effects due to a potential change in the spectral energy distribution (SED) between quiescent and bursting parts of the light curve, which would affect any bolometric correction. As a result, the obtained luminosity of CP Pup should be treated as a lower limit. It is, however, possible to estimate the effect the bolometric correction could have on the luminosity. The X-ray luminosity in Section 3.4 is estimated to be $L_X \sim 1.1 \times 10^{33}$ erg s^{-1}. Similarly, Orio et al. (2009) estimated the UV luminosity to be $L_{UV} \sim 2 \times 10^{33}$ erg s^{-1}. Alongside with the mean *TESS* luminosity of $L_{TESS} \sim 1 \times 10^{33}$ erg s^{-1}, the total bolometric luminosity is expected to be of the order of ∼4 $\times 10^{33}$ erg s^{-1}. Therefore, the lower limits on the luminosity are expected to represent about ∼4× lower values than the total bolometric values.

Further data used in this work have been obtained by *XMM–Newton* on 2005 June 4 and reported in Orio et al. (2009). As

---

[1] https://mast.stsci.edu/portal/Mashup/Clients/Mast/Portal.html

[2] https://docs.lightkurve.org/index.html
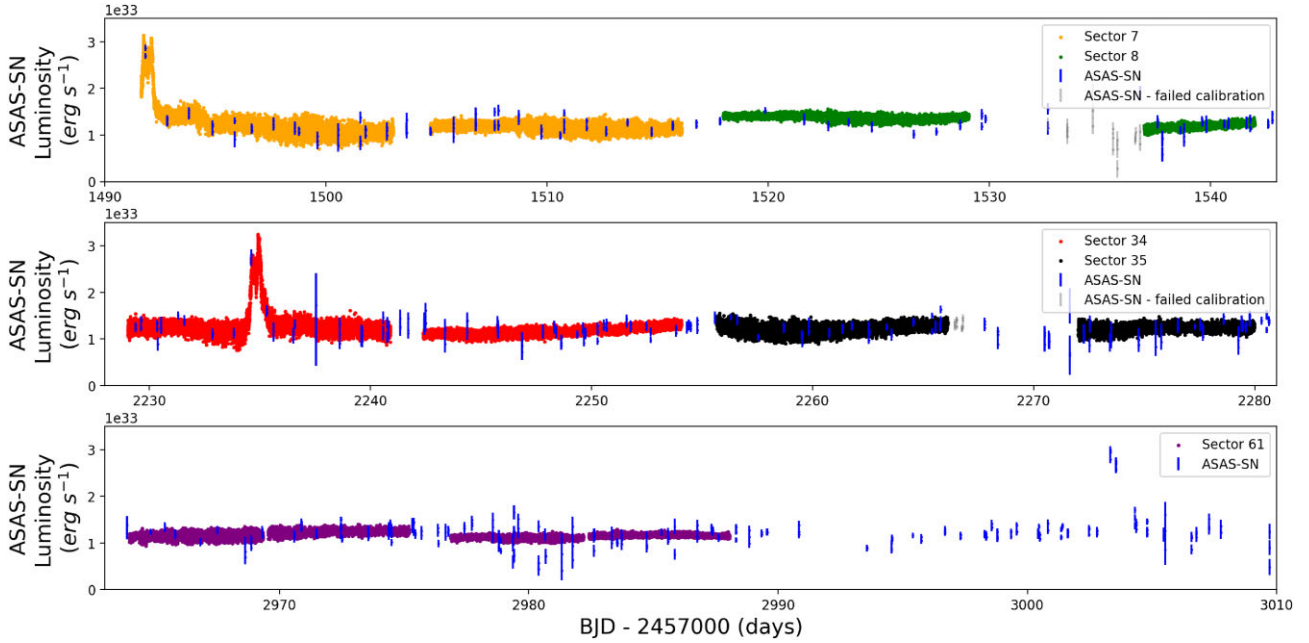[3] https://asas-sn.osu.edu/

Figure 1. Light curve of CP Pup showing all five sectors of *TESS* data as described in Table 1 (consecutively for sectors 7 and 8 in the top panel, 34 and 35 in the middle panel and 61 in the bottom panel). Overlaid is the *ASAS-SN* light curve used for calibration. The grey points are data from *ASAS-SN* for which calibration failed and hence were excluded. The flux of both *TESS* and *ASAS-SN* light curves is converted to erg s^{-1} using the *Gaia* parallax.

Table 2. Summary of the conversion coefficients from *TESS* flux in e^{-s} to *ASAS-SN* flux in mJy for CP Pup. As the conversion is done twice per *TESS* sector, all corresponding coefficients are listed.

Sector	Sector half	$A \left(\frac{mJy}{e^{-}s^{-1}} \right)$	C (mJy)
7	1	0.0241 ± 0.0007	-1.2 ± 0.1
	2	0.016 ± 0.002	-0.0 ± 0.3
8	1	0.011 ± 0.001	-0.9 ± 0.4
	2	0.011 ± 0.001	-0.9 ± 0.4
34	1	0.0209 ± 0.0008	-11.1 ± 0.5
	2	0.011 ± 0.001	-4.6 ± 0.9
35	1	0.015 ± 0.001	-2.2 ± 0.4
	2	0.014 ± 0.003	-1.8 ± 0.9
61	1	0.013 ± 0.001	-1.8 ± 0.4
	2	0.008 ± 0.002	-0.5 ± 0.7

described in greater detail in Orio et al. (2009), the data were obtained with EPIC-pn, MOS-1, and MOS-2 with ∼50 ks exposure. Grating spectrum with low signal-to-noise ratio (SNR) was also obtained with the Reflection Grating Spectrometer (RGS) and reported in Orio et al. (2009). The spectrum is shown in Orio et al. (2009) in Fig. 3. The reduced data are available online at `heasarc`.[4] However, the data reanalysed here are only the data taken with the most sensitive EPIC-pn instrument.

3 RESULTS

In this section, we report the bursts found in two of the five available *TESS* sectors in Section 3.1. We further report on the observed variable cluster of frequencies found in the power spectrum of CP

Pup in Section 3.2. The *XMM–Newton* spectrum reported in Orio et al. (2009) and our new model fit are presented in Section 3.4

3.1 Bursts

The *TESS* light curve from all sectors is displayed in Fig. 1, where two bursts are detected in Sectors 7 and 34 with the corresponding times in Table 1. The bursts have also been reported in Bruch (2022), however, they are disregarded in the analysis. The recorded bursts in Sectors 7 and 34 all lasted ≲1 d, with the overall amplitude increasing by a factor of >2, from ∼1.5×10^{33} to >3.0×10^{33} erg s^{-1}. A detailed version of the bursts is shown in Fig. 2. Only Sector 34 contains both the immediate pre-burst and post-burst observation. Sector 7 started during the rise of the burst and contains the post-burst part only. It is worth noting an additional burst of similar nature in the long-term *ASAS-SN* light curve at ∼3005 BTJD in Fig. 1. Unfortunately, there are no *TESS* observations around that date. Another interesting characteristic of the bursts is their shape, showing two distinct peaks with ∼0.35 d separation.

To understand the origin and nature of the bursts, their energy has to be determined. This is done by integrating the luminosity under the calibrated light curve after subtracting the baseline luminosity level. We estimate the baseline luminosity using the pre- and post-burst data only. We use these to compute a running mean and interpolate in between the two with a spline function. The resulting energy in erg is reported in Table 1. The most energetic burst in Sector 7 releases in excess of 1.2×10^{38} erg. The energy released by the burst in Sector 34 is >6.3×10^{37} erg. We note that the aforementioned data gaps, as well as the lack of a bolometric correction allows us to only provide lower limits to the burst energies.

3.2 Phenomenology of the period cluster

A peculiar feature of CP Pup is the cluster of periods between ∼14 and ∼15 cycles per day (∼1.5–1.6 h). In the five *TESS*
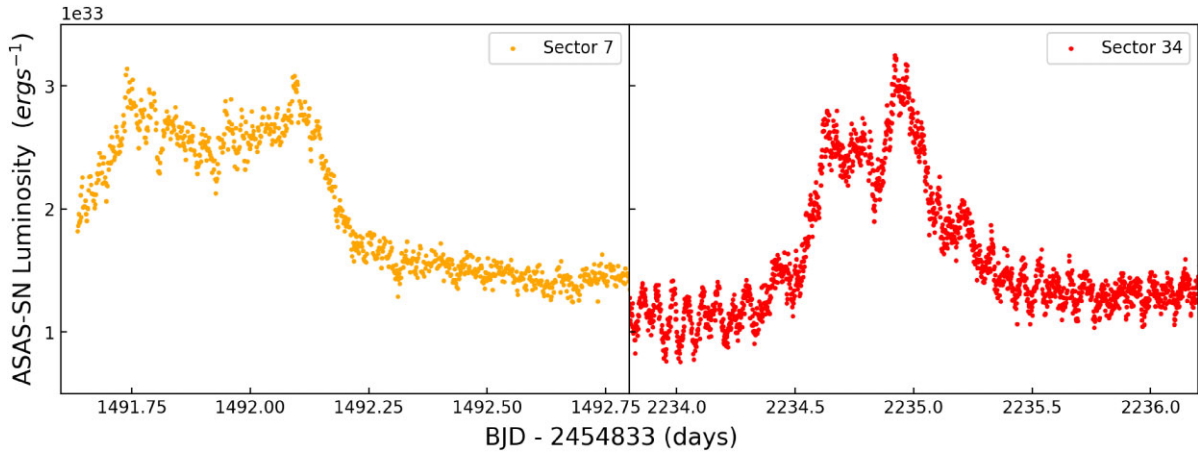
Figure 2. Zoom in on the bursts shown in Fig. 1 and described in Table 1. The energy of each burst is 1.2×10^{38} erg for sector 7 and 6.3×10^{37} erg for sector 34.
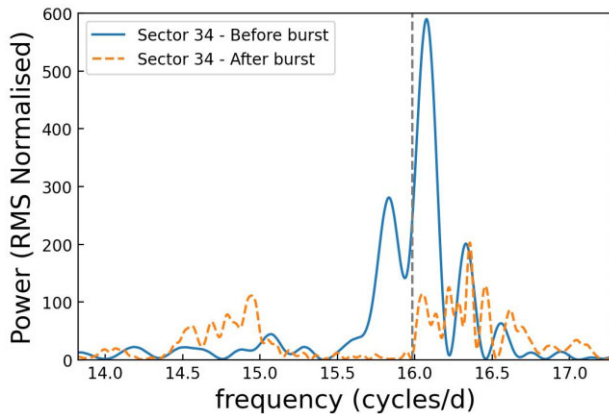

Figure 3. Power spectrum of sector 34 divided into pre-burst (solid line) and post-burst (dashed line) parts. Grey dashed line shows the coherent *XMM–Newton* period at ~16 cycles per day.

sectors reported here all show this variability. This time-dependent variability is discussed in detail in Bruch (2022). The persistent signal reported from four *TESS* sectors in Bruch (2022) is at ~16.29 cycles per day. Independently redoing the period analysis on all five *TESS* sectors also reveals a single identical persistent signal in the cluster at 16.29 ± 0.04 cycles per day.

In Fig. 3, the cluster is shown right before and after the burst present in sector 34. There is no apparent connection between the burst and the position or shift of the cluster frequencies. However, it is evident that there is considerably more rms power in the cluster before the bursts than after. For sector 34, the peak power of the cluster is at ~590 rms, whereas after burst it is at ~110 rms, excluding the power of the signal at ~16.29 cycles per day at ~200 rms. Similarly, sector 7 shows a significant quasi-periodic variability as well. However, lack of data pre-burst does not allow for similar comparison as in sector 35.

Orio et al. (2009) also report only one coherent period in the light curve of CP Pup of 16 ± 2 cycles per day (~90 min). We recover the same signal from the *XMM–Newton* data. The signal is marked by the dashed grey line in Fig. 3. Furthermore, this period also corresponds to the only persistent signal in *TESS* light curve.

3.3 The potential nature of the orbital period

The signal at 1.473 h is interpreted in literature as the orbital period of CP Pup. Using the evolutionary tracks of Knigge, Baraffe & Patterson (2011), we can estimate the temperature of the donor to be ~2700 K with radius of ~0.131 $R_\odot$ for a system with an orbital period of ~1.473 h. The corresponding WD temperature according to Knigge et al. (2011) would be 11 000 K with radius following from the WD mass in Section 3.4. In such a case, the SED of the system can be roughly approximated by two spheres radiating as blackbodies with the corresponding radii and temperatures. Another possible dominant SED component would be the accretion disc. Taking the X-ray derived accretion rate of ~1 × 10^{-10} M$_\odot$ yr^{-1} (Section 3.4) at face value, a standard Shakura–Sunyaev (Shakura & Sunyaev 1973) accretion disc from the WD surface to the tidal radius at ~0.31 $R_\odot$ is assumed. The resulting SED is hence shown in the left hand side panel of Fig. 4. It is evident that there is a deficit in flux across all observed wavebands that cannot be corrected by either an increase in accretion rate or by correcting for extinction (A_V ~ 0.6 mag, Selvelli & Gilmozzi 2019; A_H =0.107 mag and A_J =0.173 mag, Cardelli, Clayton & Mathis 1989; and A_{W1} =0.203 mag and A_{W2} =0.157 mag, Fitzpatrick 1999; Indebetouw et al. 2005).

Mason et al. (2013) discuss the possibility that CP Pup may be a long orbital period cataclysmic variable (CV). Despite no other photometric signal being detected, Mason et al. (2013) report a substantial power at low frequencies (~2.38 cycles per day). Their H β RV curve produces a fit of 9.8 h. They point out a large uncertainty of 1 d, making this a lower limit on the potential signal. The longest orbital period we can use from the evolutionary tracks of Knigge et al. (2011) at an orbital period of 5.6 h provides an estimated donor temperature of ~3900 K and radius of ~0.63 $R_\odot$. Assuming the same parameters for the WD and accretion disc as previously (with the slight correction for tidal radius being at ~0.19 $R_\odot$), the estimated SED is as shown in the right panel of Fig. 4. This is more consistent to the observed *2MASS* and *WISE* absolute magnitudes of CP Pup, suggesting a hotter and larger donor than previously anticipated. Since the evolutionary tracks in Knigge et al. (2011) do not include orbital periods above 5.6 h, the right panel in Fig. 4 represents an estimate, not a fit, of the effect a longer orbital period would have on the SED. This also tentatively suggests a longer orbital period for CP Pup than reported in the past, but a more intensive radial velocity campaign is required to unravel the problem of the orbital period of CP Pup.
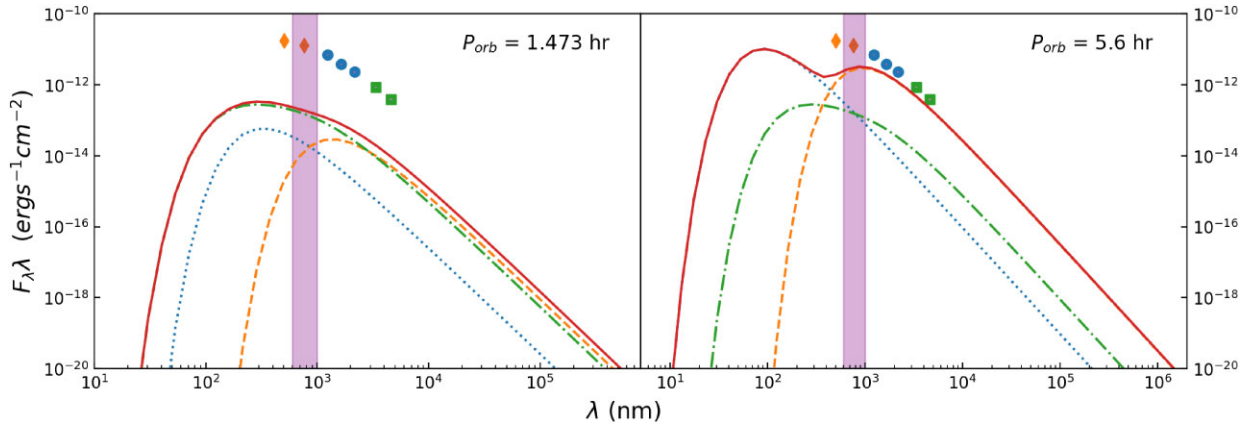
Figure 4. *Left:* model SED of CP Pup for an estimated orbital period of 1.473 h with the dotted line representing the WD, dashed line the secondary, and the dash–dotted line the accretion disc. The total SED is shown in solid line. For comparison, the measurements from *WISE W*1 and *W*2 are shown (squares) as well as the *2MASS* filters (dots) and the *Gaia* measurements (diamonds). The *TESS* bandpass is shown in the shaded region. *Right:* Same SED components and data as in the left panel but for orbital period of ∼5.6 h, the longest orbital period included in the evolutionary tracks in Knigge et al. (2011).
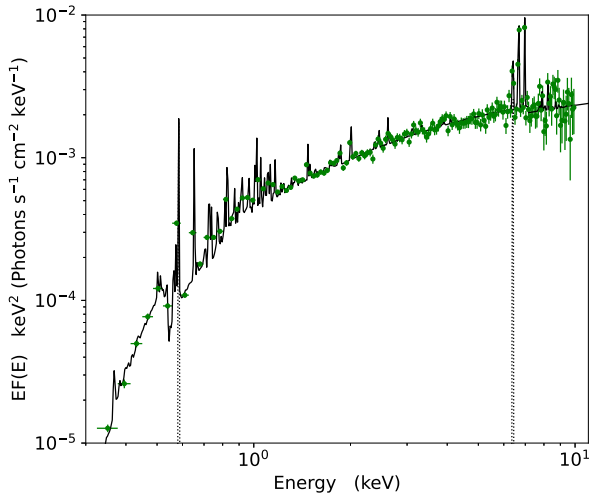

Figure 5. Unfolded XMM Epic-PN X-ray spectrum of CP Pup. The points show the data, while the solid line shows the total model. The dotted Gaussians show the two additional lines needed to fit the spectrum. These are (from left to right): O VII and Fe K α.

3.4 Revisiting the WD mass and mass accretion rate with X-rays

The reanalysis of the X-ray spectrum in this section is motivated by the inconsistent estimates of the WD maximal temperature T_{max} in the literature (Orio et al. 2009; Mason et al. 2013), leading to an uncertain WD mass and unconstrained accretion rate. This is also exacerbated by the pre-*Gaia* distances used in past X-ray analyses. More specifically, Orio et al. (2009) infer large values of T_{max} following from the used models for non-magnetic systems and a simplified model of magnetic systems. Exploring the possibility of micronova eruptions present in CP Pup, the model implemented in this work is adapted specifically for magnetic accreting WD with an accretion column.

Fig. 5 shows the archival *XMM–Newton* spectrum of CP Pup taken on 2005 June 4, reported in Orio et al. (2009). Orio et al. (2009) fit the RGS spectrum using MKCFLOW model (Mushotzky & Szymkowiak 1988) that describes the emission from a cooling multitemperature

plasma and the EPIC-pn spectrum with a multitemperature APEC model. However, their analysis does not include the combination with a complex absorber which is instead characteristic of magnetic CVs (Lopes de Oliveira & Mukai 2019; Islam & Mukai 2021) while they use a single simple absorber.

Orio et al. (2009) also use APEC multitemperature model to fit the *XMM–Newton* EPIC-pn spectrum. The APEC model consists of three temperature components and obtains a spectrum for a collisionally ionized diffuse gas. For an intermediate polar (IP) or polar, we can expect the presence of a magnetically confined accretion flow on to the magnetic pole (or poles) of the accretor. In this case, the impacting material generates a shock heated plasma, which cools towards the surface of the WD, and generates the X-ray emission. This is similar to the multitemperature APEC model used by Orio et al. (2009).

Testing the possibility that the bursts can be explained by micronova requires a magnetic accretor. Therefore, we fit the spectrum using XSPEC version 12.13.0 (Arnaud 1996), and specifically use the CEMEKL model (Singh, White & Drake 1996) that describes the emission from a multitemperature plasma. The geometry of an accretion stream on to a WD surface can be approximated as cylindrical (see fig. 1 in Done & Magdziarz 1999). X-rays emitted on the far side of the stream (with respect to the observer) encounter a larger effective column density to the observer compared to those emitted on the side facing the observer. To account for this, we convolve CEMEKL with the absorption model PWAB (Done & Magdziarz 1998), which calculates the emission assuming the non-uniform absorption profile arising from a cylindrical emitter. We further convolve the model with RELFECT (Magdziarz & Zdziarski 1995), which calculates the reflected emission from neutral material. The use of the *reflect* component follows from the presence of the Fe K α line. Additionally, we add two components to model, the fluorescence lines Fe K α (∼6.4 keV), and O VII (∼0.58 keV). The strong O VII line might be due to the wind from the nova shell, as noted in Orio et al. (2009). Finally, we also include TBABS to account for interstellar absorption as obtained from the visual extinction from table 1 in Selvelli & Gilmozzi (2019), using the optical extinction to H column density relation (Guver & Ozel 2009). The final XSPEC model is then: TBABS*PWAB*REFLECT*(CEMEKL + GAUSSIAN(FE-K α) + GAUSSIAN(O VII)). The best-fitting model is shown in Fig. 5, and the corresponding model parameters are shown in Table 3.

Table 3. The best-fitting parameters to the *XMM–Newton* EPIC-pn spectrum of CP Pup, with errors representing 90 per cent confidence limits. Values with no error were kept frozen during the fitting process, and values with no units are dimensionless. For completeness, we also include the switch parameter that were used throughout and determine whether the spectrum is computed via interpolating or pre-computed tables. The abundances used correspond to the 'angr' table (https://heasarc.gsfc.nasa.gov/xanadu/xspec/manual/node116.html).

Parameter	Units	Value
	——— TBABS ———	
N_H	$10^{22}\,cm^{-2}$	0.16
	——— PWAB ———	
$N_{h,\,min}$	$10^{22}\,cm^{-2}$	$1^{+1625}_{-1} \times 10^{-7}$
$N_{h,\,max}$	$10^{22}\,cm^{-2}$	$7.34^{+\,inf}_{-2.32}$
β		$-0.86^{+0.04}_{-0.09}$
	——— REFLECT ———	
rel_refl		$1.06^{+0.94}_{-1.04}$
Redshift		0
abund		$0.57^{+0.11}_{-0.11}$
Fe_abund		1
$\cos(i)$		0.5
	——— CEMEKL ———	
α		$0.60^{+0.10}_{-0.04}$
T_{max}	keV	$29.3^{+9.4}_{-7.4}$
n_h	cm^{-3}	1
abund		$0.57^{+0.11}_{-0.11}$
Redshift		0
switch		1
norm	10^{-3}	$5.9^{+0.9}_{-0.7}$
	——— GAUSSIAN (Fe-Kα) ———	
E	keV	6.4
EW	keV	0.07
σ	keV	10^{-2}
norm	10^{-6}	$4.56^{+1.73}_{-1.73}$
	——— GAUSSIAN (O VII) ———	
E	keV	$0.584^{+0.011}_{-0.010}$
EW	keV	0.072
σ	keV	10^{-3}
norm	10^{-5}	$2.2^{+0.4}_{-0.4}$
χ^2_ν	$148.22/159 = 0.93$	

Table 3 shows the resulting best-fitting parameters. In particular, $T_{max} = 29.3^{+9.4}_{-7.4}$ keV, significantly lower than ~ 64 keV for the multitemperature APEC model and ~ 78 keV for the MKCFLOW model discussed in Orio et al. (2009). Although T_{max} is loosely constrained, it does not approach the maximum allowed limit of the model. We attribute the main difference between this fit and that of Orio et al. (2009) to the inclusion of the PWAB component, which represents an approximation for the accretion column. Our new estimate is consistent with the range determined by Mason et al. (2013) using *Chandra* data, which has considerably softer coverage. We note that although $N_{h,\,max}$ is unconstrained its effect on the overall fit is negligible. This particular behaviour of $N_{h,max}$ is also reported in Done & Magdziarz (1998) for BY Cam. Similarly for reflection, which is loosely constrained but with negligible effect on the final value of T_{max}. The possibility of fixing reflection to 1 is also explored. It was found that a fixed value of reflection changes T_{max} to $T_{max} = 29.3^{+10.4}_{-7.1}$ keV, however, all variations of the temperature are well within the errors, making a fixed value of reflection unnecessary.

Done & Magdziarz (1998) explored the possibility of fixing $\alpha = 1$, however found that the best fit is obtained for $\alpha < 1$. This is also the case for CP Pup and is indicative of multiple sources of cooling, not only bremsstrahlung, most likely cyclotron.

To infer the WD mass and mass accretion rate, it is here assumed that CP Pup is a magnetic system. This choice was based on partial evidence as presented in Mason et al. (2013) and other works, but also in order to explore the micronova nature of the bursts. From the updated X-ray fit, we first isolate the plasma component from the model spectrum, extrapolating it over the energy range for which the model is defined ($5 \times 10^{-3} - 60$ keV) and integrating it. This results in a bolometric flux of $\sim 1.5 \times 10^{-11}$ erg s^{-1} cm-2. Using the *Gaia* inferred distance of $D = 780 \pm 11$ pc, this gives $L_X \sim 1.1 \times 10^{33}$ erg s^{-1}. The WD mass is derived from T_{max} using equation 1, relating the shock temperature to the WD mass in magnetic cataclysmic variables, in Orio et al. (2009) following from Wu et al. (2003) and references therein. The resulting mass is $M_{WD} \sim 0.73$ M$_\odot{}^{+0.12}_{-0.11}$ with the corresponding radius $R_{WD} \sim 0.011$ R$_\odot{}^{+0.001}_{-0.002}$, assuming the mean molecular weight from the abundance in Table 3.

Assuming the inferred M_{WD} is correct, we find a mass accretion rate $\dot{M} = 1 - 2 \times 10^{-10}$ M$_\odot$ yr^{-1}. The accretion rate is quite low, however, estimating the optical luminosity from *Gaia* magnitude yields $\sim 8.8 \times 10^{32}$ erg s^{-1}. Therefore, estimating the accretion rate from the optical luminosity would lead to similarly low values. As it is likely that the accretion luminosity is not solely constrained to X-rays, it is reasonable to assume that the accretion rate above is a lower limit.

Another method of estimating the accretion rate is through the optical to near-infrared SED. Using the photometric observations of CP Pup available in Vizier,[5] the peak of the SED is placed at *XMM–Newton* optical Monitor at ~ 543 nm with 2.26 ± 0.06 mJy. This translates to a luminosity of $2.53 \pm 0.02 \times 10^{33}$ erg s^{-1} using a distance of 780 ± 11 pc. Assuming that the luminosity corresponds to the accretion luminosity $L_{acc} = \frac{GM_{WD}\dot{M}}{2R_{in}}$, the estimated accretion rate is $\dot{M} \sim 6 \times 10^{-10}$ to 6×10^{-9} M$_\odot$ yr^{-1}. The range of estimated accretion rate depends on the possible truncation of the inner accretion disc. The values taken into account here estimated $R_{in} \sim R_{WD} - 10 \times R_{WD}$, where $10 \times R_{WD}$ is a value representative of the estimated truncated disc radii in IPs from Suleimanov, Doroshenko & Werner (2019) for systems of similar mass to CP Pup. Whereas this only represents a very rough estimate of the accretion rate, it corresponds to the same order of magnitude as the X-ray accretion rate. Integrating the entire available SED, with a cut-off after W_2 *WISE* band, would result in total luminosity of $\sim 4 \times 10^{34}$ erg s^{-1}. This would correspond to $\dot{M} \sim 9 \times 10^{-9}$ to 9×10^{-8} M$_\odot$ yr^{-1}, a significantly higher value than previous estimates. The excess may be accounted for if part of the SED is dominated by the donor star as suggested in Section 3.3. In such a case, the approximation of accretion luminosity through the SED peak provides a more accurate estimate.

It is important to note that we do not have sufficiently high spectral coverage to confidently determine the maximum plasma temperature, T_{max}, which sets the roll-over in the spectrum, and should therefore also affect the derived luminosity. Hence, the above estimates should be treated with caution, noting the model dependence. Furthermore, the accretion rate range above is a lower limit determined by the underlining assumptions.

[5] https://vizier.cfa.harvard.edu/vizier/sed/

Table 4. Summary of accretion rate estimates for CP Pup from literature and the parameters used to determine it. The recurrent time-scale range is computed for the ejected masses above and compared to the results in this work.

Paper	Data	Model	$T_{\max}$ (keV)	Distance (pc)	M_{WD} ($M_\odot$)	$\dot{M}_{\mathrm{acc}}$ ($\times 10^{-10}$ $M_\odot$ yr^{-1})	t_{rec} (d)	Constrained
Orio et al. (2009)	*XMM–Newton*	APEC	64	1600	>1.1	≲1.6	7.3–14	No
Mason et al. (2013)	*Chandra*	VMCFLOW	$36.5^{+19.2}_{-16.3}$	1600	$0.8^{+0.19}_{-0.23}$	4^{+3}_{-1}	1.6–6.9	Yes
Selvelli & Gilmozzi (2019)	–	Livio (1992)	–	795 ± 13	1.16 ± 0.2	$6.0^{+6.6}_{-3.1}$	0.9–7.8	–
This work	*XMM–Newton*	CEMEKL	$29.3^{+9.4}_{-7.4}$	780 ± 11	$0.73^{+0.12}_{-0.11}$	1–2	7–23	Yes

4 DISCUSSION AND CONCLUSIONS

In this section, we discuss the interpretation of the nature of the bursts detected in CP Pup. A connection is drawn in Section 4.1 with micronova, where the details of the model are discussed as well as its limitations and application to CP Pup. The recurrence time-scale is determined from the model and compared to that observed from *ASAS-SN* data. As mentioned in Section 3.4, the interpretation of the nature of the bursts, as well as the accretor mass and accretion rate are here dependent on the assumption that CP Pup is a magnetic system.

4.1 The CP Pup bursts as micronova eruptions?

The energy and shape of bursts shown by CP Pup resemble at least phenomenologically the bursts reported in Scaringi et al. (2022c) and Schaefer, Pagnotta & Zoppelt (2022). In Scaringi et al. (2022c), the bursts are interpreted as micronova bursts, somewhat analogous to Type I X-ray bursts in neutron stars. Micronovae are hypothesized to be the result of a thermonuclear runaway effect in a relatively small magnetically confined accretion column. The objects so far reported to show these bursts are TV Col, EI UMa, and ASASSN-19bh, with burst energies ranging from 9×10^{37} to 1.2×10^{39} erg. TV Col in particular has been observed at UV wavelengths during one of the bursts by Szkody & Mateo (1984), displaying high-ionization helium and nitrogen lines strengthening during the burst as well as clear P-Cygni profiles suggesting outflow velocities in excess of 3500 km s^{-1}. The bursts in TV Col and EI UMa have been compared to those in V1223 Sgr (Hameury, Lasota & Shaw 2022). In Hameury et al. (2022), the bursts reported in V1223 Sgr are interpreted by the magnetic-gating accretion instability model as observed in other accreting WDs (Scaringi et al. 2017, 2022a; Littlefield et al. 2022), but draws no definite conclusion on the nature of bursts in other IPs. Although magnetic gating may explain some observables for V1233 Sgr, it may not explain the large outflows observed by Szkody & Mateo (1984) in TV Col. The recurrent nova V2487 Oph has also been reported to display fast bursts that appear phenomenologically similar (Schaefer et al. 2022), but their interpretation has been argued to be attributed to flares due to magnetic recconection events within the accretion disc.

If these are indeed related to the micronova events, then we can attempt to compute the burned/ejected mass during one of these events. The average conversion rate of hydrogen during the CNO cycle in a standard nova explosion (Bode & Evans 2008; José, Shore & Casanova 2020) is $\approx 10^{16}$ erg g^{-1}. With this assumption the observed energies convert to ejected masses of $>6.2 \times 10^{-12}$ and $>3.2 \times 10^{-12}$ $M_\odot$ for sectors 7 and 34 respectively, somewhat lower than those reported for TV Col and EI UMa in Scaringi et al. (2022c) of 1.8–5.8×10^{-11} $M_\odot$. We note that all these estimates should be considered lower limits as no colour and bolometric corrections

have been applied. Hence the energies, and consequently ejected mass would most likely be larger under this interpretation.

From the micronova model (Scaringi et al. 2022b), the recurrence of the bursts is simply associated with the time it takes for a confined column of material to reach thermonuclear runaway conditions. In the simplest scenario, the burst recurrence time is given by $t_{\mathrm{rec}} = \frac{M_{\mathrm{ejected}}}{\dot{M}_{\mathrm{acc}}}$, where M_{ejected} represents the ejected mass during the burst and $\dot{M}_{\mathrm{acc}}$ the accretion rate of the system. The mass accretion rate estimated from the fit to the *XMM–Newton* spectra is between 1×10^{-10} to 2×10^{-10} $M_\odot$ yr^{-1}. This assumes a WD mass of $M_{\mathrm{WD}} \sim 0.73$ $M_{\odot}{}^{+0.12}_{-0.11}$, as estimated in Section 3.4. Hence, the estimated recurrence time would be $t_{\mathrm{rec}} \approx 7$–23 d. For comparison, the accretion rates quoted above from literature and the one determined in this work are all compared in Table 4 alongside with the corresponding recurrence times. Most of the accretion rates in Table 4 are also derived from fits to X-ray spectra and in such case the $T_{\max}$ and appropriate model are given as well. The table also notes if the model has a constraint on the $T_{\max}$ parameter and hence the accretion rate. This is judged by the constraint placed on the $T_{\max}$ by the model boundaries of the parameter.

The long-term *ASAS-SN* light curve may also constrain the recurrence time-scale of the bursts. Fig. 1 reveals an additional burst not observed by *TESS* after the ones detected in Sectors 7 and 34 around ~3005 BTJD. Along with the two bursts observed by *TESS* this suggests a recurrence time-scale of ~60 d. Considering the entire long-term *ASAS-SN* light curve from ~1020 BTJD to ~3020 BTJD, the recurrence time can be roughly estimated to be ~30–60 d. The lower limit of the range is consistent with the predicted recurrence time-scale using the accretion rate from Section 3.4. We do note that the data gaps could potentially make this an upper limit on the recurrence time. Beyond the long-term *ASAS-SN* data, it is difficult to estimate if the recurrence holds.

Given the 1942 classical nova eruption, it is plausible to assume that up until then the WD in CP Pup had accreted $\approx 10^{-5}$ $M_\odot$ during the preceding centuries, and that this fresh hydrogen material would be spread across the entire WD surface. On the other hand, from the *ASAS-SN* long-term light curve it appears that fast burst events have been recurring in CP Pup for at least ~4 yr. Assuming these events are indeed micronova eruptions, the amount of mass used by the micronova events would then constitute only ~0.005 per cent of the mass required to trigger the next classical nova. It is of course also possible that micronova events have been occurring since the 1942 nova explosion. In this case, the consumed mass from micronovae would represent about 0.1 per cent of the required mass to trigger the next classical nova. It is unclear how the recurrence time-scales of micronovae and classical nova in the same system relate to each other, but we point out that the two types of explosions do not necessarily need to be mutually exclusive. The magnetic confinement criteria required may not be attained for long enough time to build up enough material to trigger a micronova, allowing lateral spreading of freshly

accreted material. The exact conditions for this remain unclear and it is possible that the bursts have not always been present in the system, for example if the conditions for magnetically confined accretion are fulfilled only temporarily. In such a case one or multiple micronova may be triggered. Cessation of micronova events could happen if the magnetic confinement of the accretion column is broken. Whether the accretion column can stay magnetically confined is thought to depend on the combination of multiple parameters, such as the strength of the magnetic field, the column height and footprint area as described in detail in Scaringi et al. (2022b).

Assuming a micronova interpretation, the lower limit of the recurrence deduced from the long-term *ASAS-SN* light curve t_{rec} ≈ 30 d, the expected ejected mass would convert to ~ 3–6×10^{-11} $M_\odot$, consistent with those reported in Scaringi et al. (2022c). This, however, would imply that the released energy in the *TESS* passband underestimates the bolometric release of energy by a factor of 3 or more. It is, however, possible that lower mass transfer rates could yield consistent burst recurrence times and energies.

All the recurrence time-scales in Table 4 are, however, either shorter or on the lower boundary of the recurrence time-scale deduced from the long-term *ASAS-SN* light curve. This might be due to the number of necessary conditions for micronova to occur. For example, the magnetic pole can change the size of its footprint on the surface of the WD before enough material is accreted for a micronova to be triggered. In such a case, the recurrence time-scale would become longer. The recurrence time-scales could also be underestimated due to the WD mass. The same underestimation can be applicable in the recurrence time-scale using accretion rate from other papers, see Table 4. For the mass of the WD to be better constrained, however, a wider spectral coverage is necessary, such as that of *NuSTAR*.

Another important parameter of the micronova model is the fractional area on which material is being accumulated. From the ejected masses $M_{ejected}$, the fractional area f can be derived from fig. 1 in Scaringi et al. (2022c). For $M_{ejected}$ and WD mass quoted above, the expected f is ~ 2–9×10^{-7}. This is particularly low for triggering micronova and may point to the bombardment scenario suggested for polars (Frank, King & Raine 2002). In that case, inhomogeneous accretion of dense blobs penetrate into the WD photosphere and radiate most of their energy in a form of soft X-rays. In such a scenario in Frank et al. (2002), the accretion rate is constrained by $\lesssim 1.6 \times 10^{-11}$ $M_\odot$ yr^{-1}. This is much lower than the estimated accretion rate for CP Pup and argues against the micronova interpretation. The only way out from this potential problem with the model is that the WD mass has been underestimated in the X-ray spectral analysis.

Further photometric, polarimetric and high-time resolution spectroscopic follow-up observations, of the peculiar behaviour displayed by CP Pup will provide additional constraints to unravel its true nature. Specifically the lack of consistent results when it comes to CP Pup, coupled with the lack of a coherent model to explain its behaviour, may warrant a dedicated observing campaign.

DATA AVAILABILITY

The *TESS* data used in the analysis of this work is available on the MAST webpage https://mast.stsci.edu/portal/Mashup/Clients/Mast/Portal.html. The *ASAS-SN* data (Shappee et al. 2014; Kochanek et al. 2017) used for the calibration of *TESS* data are available on the *ASAS-SN* webpage https://asas-sn.osu.edu/.

REFERENCES

Arnaud K. A., 1996, in Jacoby G. H., Barnes J.eds, ASP Conf. Ser. Vol. 101, Astronomical Data Analysis Software and Systems V. Astron. Soc. Pac., San Francisco, p. 17
Balman S., Orio M., Ogelman H., 1995, ApJ, 449, 1993
Bianchini A., Friedjung M., Sabbadin F., 1985, Inf. Bull. Var. Stars, 2650, 1
Bianchini A., Saygac T., Orio M., Della Valle M., Williams R., 2012, A&A, 539, 1
Bode M. F., Evans A., 2008, Classical Novae, 2nd edn. Cambridge Univ. Press, Cambridge
Bruch A., 2022, MNRAS, 514, 4718
Cardelli J. A., Clayton G. C., Mathis J. S., 1989, ApJ, 345, 245
Cohen J. G., Rosenthal A. J., 1983, ApJ, 268, 689
Della Valle M., Livio M., 1998, ApJ, 506, 818
Diaz M. P., Steiner J. E., 1991, PASP, 103, 964
Done C., Magdziarz P., 1998, MNRAS, 298, 737
Done C., Magdziarz P., 1999, Nucl. Phys. B, 69, 376
Duerbeck H. W., Seitter W. C., Duemmler R., 1987, MNRAS, 229, 653
Fitzpatrick E. L., 1999, PASP, 111, 63
Frank J., King A., Raine D., 2002, Accretion Power in Astrophysics, 3rd edn. Cambridge Univ. Press, Cambridge
Gaia Collaboration, 2016, A&A, 595, A1
Gaia Collaboration, 2023, A&A, 674, A1
Guver T., Ozel F., 2009, MNRAS, 400, 2050
Hameury J. M., Lasota J. P., Shaw A. W., 2022, A&A, 664, A7
Indebetouw R. et al., 2005, ApJ, 619, 931
Islam N., Mukai K., 2021, ApJ, 919, 90
José J., Shore S. N., Casanova J., 2020, A&A, 634, A5
Knigge C., Baraffe I., Patterson J., 2011, ApJS, 194 28
Kochanek C. S. et al., 2017, PASP, 129, 104502
Littlefield C., Lasota J.-P., Hameury J.-M., Scaringi S., Garnavich P., Szkody P., Kennedy M., Leichty M., 2022, ApJ, 924, L8
Livio M., 1992, ApJ, 393, 516
Lopes de Oliveira R., Mukai K., 2019, ApJ, 880, 128
Magdziarz P., Zdziarski A. A., 1995, MNRAS, 273, 837
Marelli M., De Martino D., Mereghetti S., De Luca A., Salvaterra R., Sidoli L., Israel G., Rodriguez G., 2018, ApJ, 866, 125
Mason E. et al., 2013, MNRAS, 436, 212
Mushotzky R. F., Szymkowiak A. E., 1988, in Fabian A. C., ed., NATO Advanced Study Institute (ASI) Series C Vol. 229, Cooling Flows in Clusters and Galaxies. Springer, Dordrecht, p. 53
O'Donoghue D., Warner B., Wargau W., Grauer A. D., 1989, MNRAS, 240, 41
Orio M., Mukai K., Bianchini A., de Martino D., Howell S., 2009, ApJ, 690, 1753

Patterson J., Warner B., 1998, PASP, 110, 1026

Patterson J. et al., 2013, MNRAS, 434, 1902

Payne-Gaposchkin C., 1964, The Galactic Novae. Dover Publication, New York

Prialnik D., Kovetz A., 1995, ApJ, 445, 789

Scaringi S., Maccarone T. J., D'Angelo C., Knigge C., Groot P. J., 2017, Nature, 552, 210

Scaringi S. et al., 2022a, Nat. Astron., 6, 98

Scaringi S., Groot P. J., Knigge C., Lasota J. P., de Martino D., Cavecchi Y., Buckley D. A. H., Camisassa M. E., 2022b, MNRAS, 514, L11

Scaringi S. et al., 2022c, Nature, 604, 447

Schaefer B. E., Collazzi A. C., 2010, AJ, 139, 1831

Schaefer B. E., Pagnotta A., Zoppelt S., 2022, MNRAS, 512, 1924

Selvelli P., Gilmozzi R., 2019, A&A, 622, A186

Shakura N. I., Sunyaev R. A., 1973, A&A, 55, 155

Shappee B. J. et al., 2014, ApJ, 788, 1

Singh K. P., White N. E., Drake S. A., 1996, ApJ, 456, 766

Suleimanov V. F., Doroshenko V., Werner K., 2019, MNRAS, 482, 3622

Szkody P., Mateo M., 1984, ApJ, 280, 729

Warner B., 1985, MNRAS, 217, 1P

White J. C. II, Honeycutt R. K., Horne K., 1993, ApJ, 412, 278

Wu K., Cropper M., Ramsay G., Saxton C., Bridge C., 2003, Chin. J. Astron. Astrophys. Suppl., 3, 235

This paper has been typeset from a TeX/LaTeX file prepared by the author.